Thrombopoietin receptor agonist eltrombopag prevents insulin resistance-mediated synaptic pathology via HIF1α/GSK3β/Sirt1 pathway

He Yu
Wenzhou Medical University First Affiliated Hospital: The First Affiliated Hospital of Wenzhou Medical University

Xuebao Wang
Wenzhou Medical University Affiliated Dongyang Hospital: Dongyang People's Hospital

Leping Liu
Wenzhou Medical University First Affiliated Hospital: The First Affiliated Hospital of Wenzhou Medical University

Baihui Chen
Wenzhou Medical University First Affiliated Hospital: The First Affiliated Hospital of Wenzhou Medical University

Shuya Feng
Wenzhou Medical University First Affiliated Hospital: The First Affiliated Hospital of Wenzhou Medical University

Xiaoai Lu
Wenzhou Medical University First Affiliated Hospital: The First Affiliated Hospital of Wenzhou Medical University

Ruimin You
Wenzhou Medical University First Affiliated Hospital: The First Affiliated Hospital of Wenzhou Medical University

saidan ding (firstdsdan@hotmail.com)
Wenzhou Medical University

Research

Keywords: insulin resistance, thrombopoietin receptor agonist eltrombopag, cognitive decline, HIF1α/GSK3β/Sirt1 pathway, minimal hepatic encephalopathy

DOI: https://doi.org/10.21203/rs.3.rs-153170/v1

Abstract

Background

Minimal hepatic encephalopathy (MHE) is characterized by impaired cognitive function and memory loss, which are often the result of synaptic pathology. Insulin resistance has been reported to be closely correlated with the pathogenesis of MHE.

Methods

The effect of thrombopoietin receptor agonist eltrombopag (ELT) on neurodegeneration and insulin resistance was examined in the primary rat neurons and an MHE rat model.

Results

We found that the level of thrombopoietin receptor c-MPL (MPL) expression was decreased in MHE brains, and ELT administration improved insulin resistance, alleviated the destruction of synaptic formation and enhanced learning and memory in the MHE rats, indicating the relationship between dowregulated ELT and insulin resistance. Then in vitro, ELT treatment ameliorated the impairment of glucose uptake, indicating the reduction of insulin resistance. High dose of glucose inhibited insulin-stimulated downregulation of Hypoxia-inducible factor-1α (HIF1α) expression, the phosphorylation of GSK3β (pGSK3 β), upregulation of sirtuin-1 (Sirt1), destruction of synaptic formation and activity, which were all reversed by ELT treatment in insulin resistant neurons.

Conclusions

These results indicate that ELT is a promising potential therapeutic agent for insulin resistance and defect in learning and memory.

Introduction

Thrombopoietin (TPO), a stimulator of megakaryocytic/platelet lineage, acts in the brain as a counterpart of erythropoietin (EPO), a hematopoietic growth factor with neuroprotective properties. TPO and its receptor c-MPL (MPL) are expressed in the neurons of the human central nervous system (CNS) and murine neural cells. TPO is prominent in human cerebrospinal fluid 1. TPO was found to be neuroprotective in the CNS in hypoxic-ischemic neonatal rat brain models. TPO reduced brain damage and improved sensorimotor functions. In addition, TPO had a stimulating effect on neural cell proliferation and exerted an antiapoptotic effect 2 3. TPO improved neurological function and ameliorated brain edema after stroke 4. In the developing human CNS, the thrombopoietin gene is abundantly expressed. Considering that thrombopoietin contains a neurotrophic sequence, it may well

play a role in neuronal cell biology 5. Prior to the isolation of TPO, its receptor was identified as the cellular proto-oncogene targeted by murine myeloproliferative leukemia virus and was therefore named MPL. Importantly, TPO and its receptor MPL are expressed in the neurons of the human central nervous system (CNS) and murine neural cells 5–8. TPO is prominent in human cerebrospinal fluid 1.The biological actions of TPO are initiated by specific binding to its receptors (i.e., MPL) that are expressed on the surface of target cells. Signal transduction from activation of the MPL receptor following TPO binding has been demonstrated in many cell types. Minimal hepatic encephalopathy (MHE) is characterized by a mild impairment in cognition and psychomotor skills, which further progress to a gross impairment in orientation and general consciousness 9,10.Thus, impaired TPO signaling is critical for the development of cognitive deterioration in the brain, suggesting that TPO replacement therapy might prevent cognitive disturbance in MHE. Eltrombopag (ELT) is an orally active small molecule thrombopoietin receptor agonist 11. However, the effect of ELT on cognitive function in MHE remain largely unknown.

Hypoxia-inducible factor-1α (HIF1α) is highly expressed in the adipose tissues of obese individuals and decreases after weight loss 12. It has been reported that adipocyte-specific HIF1α overexpressing mice develop insulin resistance 13. Deletion of HIF1α in adipocytes protects mice from HFD-induced insulin resistance 14,15. HIF1 is a hetero-dimer consisting of the oxygen regulated HIF1α subunit and the constitutively expressed Hypoxia-inducible factor-1β (HIF1β) subunit 16. HIF1α is a master regulator of hypoxic responses. Under hypoxic environments, HIF1α subunit is translocated from the cytoplasm to the nucleus, where it dimerizes with the HIF1β subunit and activates the transcription of genes that are required for hypoxic biological responses, including neoangiogenesis and adaptive glucose metabolism 17. We hypothesized that HIF1α was critically involved in the neuronal insulin resistance. It was suggested that poor cognitive performance in MHE individuals was associated with insulin resistance that regulates learning and memory function via an increased HIF1α expression.

In our previous study, we have demonstrated that insulin resistance was presented in MHE and was associated with the pathogenesis of MHE 18. In the present study, we tested whether insulin resistance was linked to impairment in learning and memory in MHE accompanied by reduced ELT expression, and whether ELT improved cognitive decline and insulin resistance. This study was aimed at establishing the insulin resistance -mediated HIF1α signaling which signaled to the downstream Glycogen synthase kinase-3(GSK3 β)/sirtuin-1(Sirt1) pathway. However, the underlying mechanisms of memory impairment in MHE was complicated, and here we reported that chronic treatment with ELT protected against the deterioration of recognition and spatial memory in the MHE rat model via the amelioration of insulin resistance.

Materials And Methods

MHE models and treatments

A total of 40 Sprague-Dawley rats (experimental animal center of the Chinese Academy of Sciences in Shanghai) weighing 220-250 g were used. All experiments were carried out in accordance with the

guidelines laid down by the Ethics Committee of the First Affiliated Hospital of Wenzhou Medical University regarding the care and use of animals for experimental procedures. Before experimentation, all animals underwent two behavioral tests: Y-maze (YM) and water-finding task (WFT). Normal values for these behavioral tests were obtained. Rats were then randomly divided into two groups: a control group (n=20) and a thioacetamide (TAA) treated group (n=30). Liver cirrhosis was induced by intraperitoneal injection (i.p.) of TAA (200 mg/kg in normal saline, Sigma-Aldrich) twice per week for 8 weeks. TAA-treated rats were diagnosed as hepatic encephalopathy (HE) based on the following symptoms: later development of decreased motor activity, lethargy, and eventual progression to coma. TAA-treated rats with no HE symptoms were subjected again to behavioral tests to confirm whether MHE had developed. If TAA-treated rats met the alternative criteria for MHE as follows, they were included in the MHE group: a) values of YM lower than mean ± 1.96·SD; b) values of WFT higher than mean ± 1.96·SD 19. For Thrombopoietin receptor agonist eltrombopag (ELT, Selleck Chemicals #S2229) administration, MHE rats were conducted oral administration (0,5,25mg/kg).

YM test

Rats were individually placed at the end of an arm and allowed to explore the maze freely for 8 min. Total arm entries and spontaneous alternation percentage (SA%) were measured. SA% was defined as the ratio of arm choices that differed from the previous two choices (‘successful choices’) to total choices during the run (‘total entry minus two’, because those two entries could not be evaluated) 20.

WFT test

A rat was placed at the near-right corner of the apparatus and allowed to explore it freely for 3 min. Rats were omitted from the analysis when they could not find the tube within the 3-min exploration. After the training session, rats were deprived of water for 24 h. In the trial session, rats were again individually placed at the same corner of the apparatus and allowed to find and drink the water in the alcove. The elapsed times until the entry into the alcove (entry latency, EL), until the touching/sniffing/licking of the water tube (contacting latency, CL) and until the initiation of drinking from the water tube (drinking latency, DL) were measured 21.

Primary hippocampal neurons (PHNs) culture and treatments

The hippocampus was dissected from 14 d gestation Sprague-Dawley rat embryos and placed in ice cold Hank’s buffered salt solution (HBSS). Tissues were incubated with 0.25% trypsin in HBSS for 5 min in 37 °C/5% CO2. Cells were dissociated by trituration through a glass Pasteur pipet and then passed through a 70 μm cell strainer (Falcon 352350). Cells were plated at a density of 200,000 cells/well onto poly-D-lysine/laminin-coated 8-well chamber slides in DMEM + 10% HIFBS +1% glutamine +1% Pen-Strep and incubated for 2 h. The medium was aspirated after 2 h and then replaced with selection medium (DMEM +2.75% SATO serum +1% glutamine+1% Pen-Strep) as described. Cultures were incubated in the selection medium for 5 days, and the medium was changed daily to remove dead cells.

Then cells were pre-treated with HIF1α antagonist YC-1 (10μM), HIF1α agonist DMOG (0.5 mM), GSK3β antagonist LiCl (1 mM), Sirt1 agonist resveratrol (100 μM), or Sirt1 antagonist nicotinamide (NAM, 3mM) alone or after preincubation with three concentrations of ELT (0, 6.25, 12.5 and 25 μM). After the preincubation period, the cells were stimulated with 100 nM insulin in the presence of normal (5.5mM) or high (30mM) concentration of D-glucose for 24 h.

Assessment of insulin resistance

To induce insulin resistance, primary hippocampal neurons (PHNs) were starved in serum-free DMEM medium with 0.5% (w/v) bovine serum albumin (BSA) for 3 h and pre-treated with normal (5.5mM) or high (30mM) concentration of D-glucose in 10% fetal bovine serum (FBS) DMEM. To evaluate insulin resistance, ^{3}H-2-DG radioactivity taken up by the cells was determined by a scintillation counter. high D-glucose –treated cells showed a significantly lower radioactivity than normal D-glucose -treated cells and were considered to be insulin resistant. These insulin-resistant cells were used for the following experiments.

^{3}H-2-DG uptake measurement

This assay was performed using a modified version of a previously described protocol [10]. Briefly, insulin-resistant cells were starved in serum-free, 0.5% (w/v) BSA DMEM for 3 h before treatment. To confirm insulin resistance, 100 nM insulin was added to the medium for 30 min and then the radioactivity of ^{3}H-2-DG taken up by the cells was determined. To investigate the effects of ELT on glucose uptake or insulin-stimulated glucose uptake, various concentrations of ELT were added to the medium alone or followed by 100 nM insulin for 30 min. To determine the involvement of the HIF1α/GSK3β/Sirt1 pathway, the 10μM YC-1, 0.5mM DMOG, 1mM LiCl, 100μM resveratrol or 3mM NAM was added to the medium 30 min before ELT treatment, respectively. After washing three times with Krebs–Ringer phosphate buffer (KRP, 1.32 mM NaCl, 4.71 mM KCl_2, 47 mM $CaCl_2$, 1.24 mM $MgSO_4$, 2.48 mM Na_3PO_4, and 10 mM HEPES (pH 7.4)), a final concentration of 1 μCi/ml ^{3}H-2-DG was added to the cells. The medium was aspirated 10 min later, and the cells were washed three times with icecold KRP to terminate the reaction. Next, the cells were lysed with 0.1 N NaOH, and the radioactivity taken up by the cells was determined using a scintillation counter (LS 6500, Beckman Instruments, Fullerton, CA, USA). Nonspecific glucose uptake was measured by subtracting values for ^{3}H-2-DG in the presence of 100 nM cytochalasin B.

Detection of fasting glucose and insulin levels

After the behavior tests, the rats fasted for 12 h, 3 ml of blood samples were collected from each rat and centrifuged at 1200×g, 15min to abtain the serum. The fasting blood glucose levels were determined by a glucose-oxidase biochemistry analyzer and fasting insulin levels were measured by homogeneous phase competitive immunoradiometric assay with an immunoreagent kit using a GC-911c immunoradiometric counter (Enterprises Group of USTC, Hefei, China). The homeostasis model of insulin resistance (HOMA-IR) was calculated using the formula: [fasting glucose (mmol/l) × fasting insulin (IU/mL)]/22.5.

Dendritic spine density analysis in primary neurons

Neural dendritic spine analysis was performed by immunocytochemistry with anti-microtubule-associated protein 2B (anti-MAP2B) and anti-vesicular glutamate transporter 1 antibodies. After fixation, neurons were incubated with primary antibodies anti-MAP2B (MAP2B; 1:200; BD Transduction Laboratories, San Jose, CA, USA) and anti-vesicular glutamate transporter 1 (vGlut1; 1:100; Neuromab, Davis, CA, USA) overnight at 4°C. Cells were then washed with PBS, incubated with secondary antibody conjugated with AlexaFluor conjugates (1:500; Life Technologies, Waltham, MA, USA) for one hour at room temperature, and coverslipped. A Z stack of optical section was visualized on a confocal laser scanning microscope (FV10i-w, Olympus, Tokyo, Japan). At least 10 cultured neurons from 2 batches of cultures per group were used for quantitative analysis.

Functional labeling of presynaptic boutons with FM4-64

FM4-64 staining (Invitrogen) was performed according to the manufacturer's instructions. Briefly, primary neurons were incubated with 5 mg/mL FM4-64 (Invitrogen) and 50 mM KCl in HBSS for 1 min at 4°C, and washed with HBSS to remove free FM4-64.

Reverse transcription-polymerase chain reaction (RT-PCR) and Quantitative Real-time PCR (qPCR)

Total RNA was isolated using the Qiagen RNeasy kit (Hilden, Germany) according to the manufacturer's protocol. cDNA was created using oligo (dT), dNTP, 0.1 M DTT, Moloney murine leukemia virus reverse transcriptase, RNaseOUT, and 5× FS Buffer (all from Invitrogen). For RT-PCR, cDNA was amplified with PCR Master Mix (Promega, Madison, WI, USA). Amplified products were electrophoresed on 2% agarose gels, visualized by EtBr staining, and normalized to GAPDH. For qPCR, mRNA expression was measured by quantitative PCR using SYBR Premix ExTaq and an MX3000 instrument. PCR was performed in a reaction that included 5 μl 2× PCR master mix, 0.5 μl forward primer (10 μM), 0.5 μl reverse primer (10 μM), 2 μl cDNA. The qPCR condition was as follows: an initial denaturation step of 10 min at 95°C; 40 cycles of 95°C for 10 s, 60°C for 60 s, and 95°C for 15 s; and a final step of slow heating from 60°C to 99°C. All samples were normalized to GAPDH to calculate relative mRNA concentrations.

The primers (Invitrogen) for the murine genes were as follows:

TPO,5'GGTGGACTTCCTCCTTCTCC3'(Forward) and 5'TCGCTAGCTGCTCTGATGAA3'(Reverse); MPL,5'CCTACTGCTGCTAAAGTGGCAA3'(Forward) and 5'CAATAGCTTAGTGGTAGGTAGGA3'(Reverse); HIF1α, 5'CGTTCCTTCGATCAGTTGTC3' (Forward) and 5'TCAGTGGTGGCAGTGGTAGT3' (Reverse); Sirt1, 5'GCCATCGCAAACTTGAACCACC3' (Forward) and 5'CGTCCGCCA TCTTCCAACTGC3' (Reverse); GSK3β, 5'GACGTCCGTGATTGGCTC3' (Forward) and 5'AGCCCAGAGCCCTGTCAG3' (Reverse); Synaptotagmin, 5'CGGCAAACT GACTGTCATTC3' (Forward) and 5'GCCCCAGTGCTGTTGTAACCA3' (Reverse); neuroligin1, 5'TGCCATCAACAGACATCACTC3' (Forward) and 5'TCTACCGAGAAGGGACTTGG3' (Reverse).

Immunoblotting

Cerebral cortex tissues or PHNs were harvested in a lysis buffer (Sigma-Aldrich). Samples (50 μg protein) were separated by SDS-polyacrylamide gel electrophoresis (PAGE) and electroblotted to PVDF membrane, which was blocked by incubation in 5% non-fat dry milk dissolved in tris buffered saline-Tween (TBS-T) (150 mM NaCl, 50 mM Tris, 0.05% Tween 20). Following transfer, proteins were probed using a primary antibody: MPL, TPO, HIF1α, HIF1β, GSK3β, pGSK3β, Sirt1, synaptotagmin, neuroligin1, GDNF, PDGF and β-actin (Santa Cruz, CA, USA). Then horseradish peroxidase-conjugated anti-rabbit secondary antibody was used to detect the primary antibodies. After extensive washing, protein bands detected by antibodies were visualized by ECL reagent (Pierce, Rockford, IL, USA) after exposure on Kodak BioMax film (Kodak).

Immunofluorescence staining, immunohistochemistry and cytochemistry

Frozen brain sections or PHNs cultured on glass coverslips were fixed with 4% paraformaldehyde and then treated with 0.1% Triton X-100 at room temperature. Blocking was with PBS containing 5% normal goat serum for 1 h at room temperature. Sections were then incubated overnight at 4°C with the following primary antibodies: HIF1α, GSK3B, pGSK3β, Sirt1, synaptotagmin, neuroligin1, tyrosine hydroxylase (TH) (Abcam, Cambridge, MA, USA). Binding of primary antibodies was detected by incubating the sections for 30 min with Alexa Fluor 488 (green)/Alexa Fluor 594 (red) conjugated secondary antibodies (Abcam).

Statistical analysis

All of the data were expressed as mean ± SD. Data comparisons were analyzed using one-way analysis of variance (ANOVA). All of the data were tested in normal distribution and equal variances, when Back-of-the-envelope test was used to verify the normal distribution, and F-test was applied for determining the equality of variances. Dunnett's post hoc multiple comparison test was applied when significant differences were determined by the ANOVA model. Then P values were made for adjustment by Bonferroni correction. The level of significance was determined by $P < 0.05$ or $P < 0.01$. All analyses were performed with SPSS 18.0 (PASW Statistics 18.0).

Results

ELT decreased HIF1α expression in insulin resistant PHNs

We first determined the effect of ELT treatment on high concentration of D-glucose-induced insulin resistance in vitro by evaluating the glucose uptake by PHNs. Under low dose of D-glucose condition, insulin stimulated glucose uptake by PHNs compared to the basal condition (Figure 1a). However, under high dose of D-glucose circumstance, insulin slightly but significantly triggered glucose uptake as compared with the basal condition; Moreover, insulin failed to stimulate glucose uptake compared to low concentration of D-glucose group (Figure 1a). ELT treatment strongly triggered insulin-mediated glucose uptake in a dose-dependent manner under high dose of D-glucose state (Figure 1a). These data indicated that ELT ameliorated insulin resistance.

HIF1α plays an important part in the pathophysiology of systemic insulin resistance 22. Thus, we detected whether ELT treatment acted on the insulin resistance-induced HIF1α activity. Insulin stimulated a significant decrease over the basal level in the HIF1α in PHNs under low concentration of D-glucose condition (Figure 1b). However, under high concentration of D-glucose condition, insulin was able to mildly but obviously decrease HIF1α expression (Figure 1b). ELT treatment caused a dose-dependent decrease in insulin-stimulated HIF1α levels (Figure 1b). Through IF staining, we also confirmed hat high ELT treatment tesulted in an obviously decreased fluorescence intensity of HIF1α stimulated by insulin in insulin resistant PHNs (Figure 1c). Through RT-PCR (Figure 1d) and qPCR (Figure 1e), we found that under normal dose of D-glucose state, insulin obviously decreased the HIF1α mRNA levels compared to the basal condition, but caused a slight but significant decrement of HIF1α mRNA levels under high dose of D-glucose condition; however, high ELT treatment further induced a significant increment in HIF1α mRNA level.

As expected, high ELT treatment triggered insulin-mediated glucose uptake under high dose of D-glucose condition, treatment of YC-1 stimulated further elevation of glucose uptake, and treatment of DMOG caused blockade of the effect in PHNs (Figure 1f). For PHNs , in the case of normal concentration of D-glucose, insulin had no effect on the HIF1β level compared to the basal condition. However, under high concentration of D-glucose circumstance, insulin did not alter the HIF1β levels compared to low D-glucose group and ELT treatment also had no effect on the protein level (Figure 1g). These results indicated that ELT improved insulin resistance via the downregulation of HIF1α.

ELT triggers phosphorylation of GSK3β via inhibition of HIF1α expression in insulin resistant PHNs

GSK3β overactivity is associated with insulin resistance 23. It has been proposed that the reduction of HIF1α protein was associated with GSK3β activation 24. We examined whether ELT has the effect on the insulin resistance-induced GSK3β activity in the downstream of HIF1α signal. By IB analysis of PHNs under high concentration of D-glucose condition, insulin caused mild but marked decrement of GSK3β expression and slightly but significantly phosphorylated GSK3β (Figure 4a), ELT treatment further caused a significant increase in insulin-stimulated phosphorylation of GSK3β and an obvious decrease in GSK3β levels, which were enhanced by YC-1 and reversed by DMOG (Figure 2a). Through IF staining, we also confirmed that high ELT treatment induced a significantly decreased fluorescence intensity of insulin-stimulated pGSK3β, which were reversed by DMOG in insulin resistant PHNs (Figure 2b). Through RT-PCR, we found that under high concentration of D-glucose condition, insulin caused slightly significant decrease in GSK3β mRNA levels, and high ELT caused a marked decrease in GSK3β mRNA level in insulin-resistant PC12 cells, which were enhanced by YC-1 addition and reversed by DMOG (Figure 2c). ELT treatment obviously triggered insulin-mediated glucose uptake in PHNs under high concentration of D-glucose condition, which was amplified by pretreatment of LiCl (Figure 2d). These results indicated that ELT stimulated phosphorylation of GSK3β to inhibit insulin resistance.

ELT increased Sirt1 expression by inhibiting HIF1α/GSK3β signaling in insulin resistant PHNs

Sirt1 has been demonstrated to improve insulin sensitivity 25. Moreover, Sirt1 is essential for maintenance of normal synaptic and cognitive functions 26-28. We then addressed the effect of ELT on the insulin resistance-induced inhibition of Sirt1 expression at the downstream of HIF1α/GSK3β signaling. As indicated by figure 3a, under high concentration of D-glucose condition, insulin incubation triggered a slightly significant increment of Sirt1 expression in PHNs, and ELT addition caused a remarkably significant increase in Sirt1 levels, which was enhanced by YC-1 or LiCl and reversed by DMOG. We also confirmed by IF staining that high ELT treatment induced a significant increase in the insulin-stimulated Sirt1 fluorescence intensity, which was reversed by DMOG in high glucose-induced insulin resistant PHNS (Figure 3b). Through q-PCR, we found that under high concentration of D-glucose condition, insulin caused a slight but significant increment of Sirt1 mRNA levels in PHNS. High ELT treatment further significantly increased insulin-stimulated Sirt1 mRNA level, which was enhanced by the administration of YC-1 or LiCl and reversed by DMOG (Figure 3c). Pretreatment of resveratrol caused further elevation of insulin-mediated glucose uptake induced by ELT treatment, and pretreatment of NAM caused blockade of the effect in high glucose-induced insulin resistance in PHNs (Figure 3d). These results indicated ELT ameliorated insulin resistance via upregulation of Sirt1.

ELT has the effect on insulin-stimulated synaptic formation via HIF1α/GSK3β/Sirt1 signaling in insulin resistant PHNs

Next, we addressed the mechanism of the effect of ELT on the insulin resistance –induced impairment of synaptic formation. As determined by IB analysis for PHNs under high concentration of D-glucose, insulin treatment caused a slight but significant increment of expressions of synaptotagmin and neuroligin1 (Figure 4a), and ELT treatment caused vastly significant increases in insulin-mediated synaptotagmin/neuroligin1 levels, which was enhanced by pretreatment of YC-1, LiCl or resveratrol (Figure 4a). High ELT treatment also induced vastly obvious increases in insulin-stimulated GDNF/PDGF levels, whearas pretreatment of DMOG or NAM reversed the two proteins levels in high glucose-induced insulin resistant PHNs (Figure 4b). RT-PCR showed that, under high concentration of D-glucose condition, ELT treatment caused the vastly significant increase in insulin-stimulated synaptotagmin mRNA level in PHNs, which was enhanced by pretreatment of YC-1, LiCl or resveratrol (Figure 4c). We also found that high ELT treatment also caused the exceedingly obvious increase in insulin-stimulated neuroligin1 mRNA level, whearas pretreatment of DMOG or NAM reversed the protein levels in insulin resistant PHNs (Figure 4d).

Double IF staining with anti-vGluT1 (for staining dendritic spines) and anti-MAP2B (for staining microtubules) antibodies revealed that ELT treatment significantly increased insulin-stimulated vGluT1-positive signals in insulin-resistant PHNS cells, whearas pretreatment of DMOG or NAM reversed this reaction (Figure 4e and f). Using FM4-64 dye to probe activity-dependent synaptic vesicle recycling revealed that high ELT treatment seriously increased insulin-stimulated synaptic activity in insulin-resistant PHNS cells, which was reversed by DMOG or NAM (Figure 4g and h). These results suggest that ELT facilitated insulin resistance-impaired synaptic formation.

ELT increased MPL expression in MHE rats

We examined MPL expression in the brain tissues of the MHE rats. RT-PCR and qPCR showed reduced MPL transcription levels in cortex of MHE rats (FigureS1a and b) and decreased TPO mRNA in hippocampus of MHE rats (Figure S1c and d). These results suggest that MPL was negatively associated with pathogenesis of MHE. Then the effect of ELT on the MPL expression was addressed. Based on immunoblotting, the cortex (Figure 5a) of the MHE rats displayed significant reductions in the MPL level, which were rescued by ELT administration, whereas, the decrease in TPO levels in hippocampus of the MHE rats was also blocked by ELT administration (Figure 5b).

ELT administration improved memory impairment and insulin resistance in MHE rats

Next, we tested the effect of ELT administration on cognitive decline of MHE rats in vivo. In the YM test, the SA% of MHE rats was obviously lower than that of control rats, and the decrease was reversed by high dose of ELT administration (Figure S2a). In the WFT test, the significant increases in EL, CL, and DL of MHE rats were recovered to the normal level by administration of high dose of ELT (Figure S2b). These results suggest that the ELT improved the cognitive deficit.

Our previous study reported that insulin resistance was involved in memory disorder in MHE18. We hypothesized that the downregulation of ELT played roles in insulin resistance in the MHE rats. Therefore, the impact of ELT on the insulin resistance was tested. As seen from Table 1, for plasma in MHE rats, not only was the level of fasting glucose obviously elevated, but the insulin level was also markedly elevated, which were both reversed by high ELT administration; and the evaluation of insulin sensitivity by the HOMA-IR index showed that high ELT administration significantly reduced the HOMA-IR index. These data indicate that the ELT has the ability to ameliorate insulin resistance.

ELT decreased HIF1α expression and increased Sirt1 expression in vivo

Next, we investigated the effect of ELT on the HIF1α and Sirt1 expression in MHE rats. As shown in Figure 6a, the increased HIF1α level and decreased Sirt1 level were observed in the cortexes of MHE rats, and administration of a high dose of ELT significantly restored the expression of the protein. However, a low dose of ELT had no effect on the protein level in MHE rats. IB analysis showed the increase in HIF1α protein level and decrease in Sirt1 level in the hippocampi of MHE rats, and high ELT reversed the changes of the two proteins (Figure 6b). Using IF staining demonstrated that the decrease in Sirt1 fluorescence intensity was blocked by high ELT administration in the cortices of MHE rats (Figure 6c). We also confirmed that high ELT recovered the increased HIF1α fluorescence intensity to the normal level in the hippocampi of MHE rats (Figure 6d). These results confirm that ELT has the protective effect on the HIF1α/Sirt1 signaling in MHE.

ELT increased synaptic formation in vivo

We then tested the effect of ELT on the synaptogenesis in MHE rats. We also observed the reduction of synaptotagmin/neuroligin1 expression in the cortexes of MHE rats, whereas high ELT administration

inhibited the reduction of the two proteins dose-dependently (Figure 7a). The hippocampi of MHE rats showed decreased protein levels of GDNF/PDGF, which were also abrogated by high ELT (Figure 7b). As shown by IF staining, high ELT administration increased neuroligin1 fluorescence intensity in the cortices of MHE rats (Figure 7c). The strong immunofluorescence of synaptotagmin was induced in the hippocampi of MHE rats after ELT (Figure 7d). These results suggest that ELT has the ability to improve the deterioration of synaptogenesis in MHE.

Discussion

Thrombopoietin (TPO), a 70-kDa glycoprotein, is the primary regulator of megakaryopoiesis and the primary hematopoietic growth factor responsible for platelet production 29. TPO shows significant homology with EPO (23%) at the amino-acid level and with neurotrophins (e.g., the highest homology with BDNF, 36%) in the N-terminal region 30. MPL is predominantly expressed on megakaryocytes, mature platelets, and a subset of CD34 hematopoietic stem cells 31. Importantly, both Tpo expression and cMpl expression have also been detected in nonhematopoietic tissues, including the brain 5–8. TPO was found to be neuroprotective in the CNS in hypoxic-ischemic neonatal rat brain models. TPO reduced brain damage and improved sensorimotor functions. In addition, TPO had a stimulating effect on neural cell proliferation and exerted an antiapoptotic effect 2,3. TPO improved neurological function and ameliorated brain edema after stroke 4. In the developing human CNS, the thrombopoietin gene is abundantly expressed. Considering that thrombopoietin contains a neurotrophic sequence, it may well play a role in neuronal cell biology5. Little is known about the relationship between MPL and neuron protection, synaptic plasticity, and memory function. We found the downregulation of MPL in MHE rats. We uncovered that ELT administration facilitates upregulation of MPL. Our results indicate that MPL plays an important role in cellular mechanisms underlying synaptic formation in MHE rats. In our previous study, we have demonstrated that insulin resistance was presented in MHE and was associated with the pathogenesis of MHE 18. Insulin resistance combined with reduction of MPL level contributed to the pathogenesis of MHE. In the current study, the results indicated that the insulin resistance occurred in MHE rat brains and cognition impairment was reversed after ELT administration. Finally, MPL and TPO were recently speculated to contribute to insulin resistance-mediated pathogenesis of MHE.

The relationship between brain tissue-specific HIF1α and insulin resistance has been explored 14,15. Our results indicate that insulin resistance-induced HIF1α activation plays a key role in cognitive impairment. Insulin resistance could inhibit synaptic formation by altering the HIF1α activity. ELT is able to potently modulate insulin resistance-mediated HIF1α activity. This study also showed a linear relationship between insulin resistance and ELT reduction, and between ELT expression and cognitive functions. Our present study demonstrated that ELT is involved in regulating glucose uptake and synaptic formation via HIF1α signaling pathway. Our experiments provide evidence that the activation of HIF1α signaling is closely related to insulin resistance-regulated synaptic activity, and this effect was reversed by ELT. In this study, we identified HIF1α as a primary downstream effector of insulin resistance, essential for the signaling of synaptic formation. Our study evaluated the ability of insulin resistance to modulate the

activity of HIF1α signaling as this is a potential mechanism for insulin resistance-induced downregulation of synaptic proteins. Thus, HIF1α signaling may represent an important target for insulin resistant signaling, and ELT could modulate insulin resistance by altering HIF1α state.

GSK-3, a serine/threonine kinase that consists of highly homologous α-and β-isoforms 32, functions to phosphorylate and inactivate glycogen synthase (GS) 33,34. Therefore, GSK3β is a distal element of the insulin signaling pathway as a potential negative modulator of tissue insulin action on GS and, potentially, on glucose transport activity and as a site of intervention in insulin-resistant states 35. GSK3β plays a role in the regulation of a diverse array of cellular functions, including glycogen synthesis, protein synthesis, gene transcription, and cell differentiation 35. Importantly, GSK3β overactivity is associated with insulin resistance in female obese Zucker rats 23, in male Zucker Diabetic Fatty rats, and in obese type 2 diabetic humans 36. Moreover, selective inhibition of GSK3β leads to enhanced insulin action at the whole-body level in insulin-resistant rodents 37 and in isolated skeletal muscle tissues or cells from insulin-resistant rats 38 and humans 39. GSK3β is elevated in tissues of insulin-resistant obese rodent models 40 and in skeletal muscle of obese humans 40 and type 2 diabetic humans 36. An accumulating body of evidence indicates a role of GSK3β in the development of insulin resistance and it can be a potential site of intervention for the enhancement of insulin action in insulin-resistant states in MHE rats. The process of HIF1α signals was linked to the activation of GSK3β protein 24. We reported that insulin resistance may exert its stimulant effects on GSK3β expression through the HIF1α pathway. Insulin resistance-stimulated GSK3β upregulation appears to be dependent upon the activation of HIF1α. ELT causes a transient GSK3β phosphorylation, which are sensitive to insulin, leading to the synaptic formation via HIF1α.

However, the potential role of GSK3β as a contributor to the impairment of synaptogenesis has not yet been investigated. Taken collectively, these findings are consistent with the fact that GSK3β is a potential target of inhibition for the enhancement of insulin-stimulated glucose transport and synaptic formation in insulin-resistant neuron. Insulin resistance-mediated cognitive loss is blocked by ELT via GSK3β phosphorylation and decreased GSK3β expression. Enhancement of GSK3β signaling by insulin resistance may constitute a critical mechanism modulating insulin resistance-mediated synaptic impairment and excitotoxicity. In this study, we found that ELT is involved in regulating GSK3β production which is associated with synaptic formation in MHE rat brains. We found that administration of ELT led to memory improvement in MHE rats via GSK3β. Therefore, the activation of GSK3β signaling caused by insulin resistance can have a profound effect on synaptic formation, cognitive decline and the development of MHE.

The mammalian Sir2 homologue Sirt1 is a redox-sensitive nicotinamide adenine dinucleotide+ (NAD+)-dependent deacetylase. Sirt1 plays a critical role in metabolism and anti-aging effects 41. The activation of Sirt1 has been shown to retard the aging process 42, as well as to attenuate neurodegeneration 43. A wealth of data has shown that Sirt1 plays an important role in insulin resistance and type 2 diabetes 44. Previously, a reduced hepatic Sirt1 level has been shown to lead to hepatic insulin resistance and type 2 diabetes 45. Sirt1 depletion in adipocytes inhibits insulin-stimulated glucose uptake 46. Sirt1 is regarded

as a link between metabolism and aging 47. Sirt1 overexpression or small chemical Sirt1 activators showed beneficial effects of Sirt1 activation on glucose homeostasis and insulin sensitivity 48. Sirt1 has been demonstrated to promote glucose homeostasis by enhancing beta cell function 49 and to improve insulin sensitivity in skeletal muscles 25. The most notable finding was that the Sirt1 were fully reduced by insulin resistance in vitro. Insulin resistance induced the reduction of Sirt1 production via activation of HIF1α/GSK3β. The disruption of Sirt1 was improved by ELT administration in MHE rats. We identified the reduction of Sirt1 through the reduction of ELT levels. In this study, we found that ELT is involved in regulating the Sirt1 production involved in synaptic formation in the brains of MHE rats.

Sirt1 gain-of-function is neuroprotective in models of neurodegeneration, which are relevant to Alzheimer's disease and amyotrophic lateral sclerosis (ALS), respectively 50. In the adult brain, Sirt1 can also modulate synaptic plasticity and memory formation 51. In addition to its importance during normal brain aging, Sirt1 has also been shown to ameliorate a number of neurodegenerative disorders including Alzheimer's disease 52, Parkinson's disease 53, Huntington's disease 54, motor neuron diseases 55 and multiple sclerosis 56. Sirt1 knockout animals have morphologic alterations in neuronal structure, exhibiting dendrites with decreased complexity and shorter branches by Golgi staining 57. Studies using electron microscopy to examine synaptic morphology show that inhibiting Sirt1 decreases synaptic inputs to hippocampal neurons 58. Sirt1 knockout mice have impaired hippocampal-dependent memory that is associated with decreased long-term potentiation (LTP) in the CA1 region of the hippocampus26-28. Sirt1 is indispensable for normal synaptic plasticity and memory 26–28,58. We found that ELT is a critical factor for improving insulin resistance, and that decreased ELT is associated with insulin resistance in MHE brains. We revealed that ELT may act through inhibition of HIF1α and pGSK3β, and upregulation of Sirt1 to induce synaptic formation and lead to cognitive enhancement. These findings indicate that ELT may enhance synaptic proteins under MHE conditions in which normal synapse is impaired via Sirt1.

Glial cell line-derived neurotrophic factor (GDNF) is a member of the transforming growth factor superfamily. It is a potent neurotrophic factor active on a broad spectrum of neuronal types and has neuroprotective effects in several experimental paradigms of neural injuries 59,60. GDNF has remarkable regenerative, restorative and neurotrophic effects upon nigrostriatal dopaminergic neurons 61. GDNF exposure significantly regained cognitive abilities of atrophied neurons 62. The perturbed production and activity of GDNF has been shown responsible for impaired neural regeneration observed in clinical tissues and experimental diabetic models 63, and depletion of GDNF seems to be linked the pathology, symptoms and cognitive deterioration of some neurological diseases such as Alzheimer's disease (AD) 64,65. In the present study, we obtained results showing that administration of ELT immediately facilitates memory function in MHE rats. Our finding that synaptic formation is facilitated by ELT provides compelling evidence that ELT may be critically involved in long-term memory. Our study showed that the addition of ELT induced a further increase in synaptic proteins in insulin resistant cells.

Conclusion

Taken together, our findings combined with findings that insulin resistance in vivo support that insulin resistance combined with the reduction of MPL expression might be the common mechanism for the pathogenesis of MHE. The results support our hypothesis that insulin resistance leads to a disruption of HIF1α/GSK3β/Sirt1 signal transduction pathways in events underlying memory ability, which are reversed by ELT treatment. Our findings also showed that treatment with ELT mitigated insulin resistance, dendritic spine loss, synaptic dysfunction and memory impairment in MHE rats. These findings highlight ELT as a promising potential treatment for MHE.

Abbreviations

AD: Alzheimer's disease; BCA: bicinchoninic acid; BSA: bovine serum albumin; ELT: eltrombopag; FBS: fetal bovine serum; GDNF: Glial cell line-derived neurotrophic factor; GSK3 β: Glycogen synthase kinase-3; HE: hepatic encephalopathy; HFD: high-fat diet; HIF1α: Hypoxia-inducible factor-1α;

HIF1β: Hypoxia-inducible factor-1; HOMA-IR: homeostasis model of insulin resistance; i.p.: intraperitoneal injection; KRP: Krebs–Ringer phosphate buffer; LTP: long-term potentiation; MAP2B: microtubule-associated protein 2B; MHE: Minimal hepatic encephalopathy; MPL: thrombopoietin receptor; PBS: phosphate buffer saline; PDGF: Platelet-derived growth factor; pGSK3 β: phosphorylation of GSK3β;

PHNs: Primary hippocampal neurons; qPCR: Quantitative Real-time PCR; RT-PCR: Reverse Transcription-Polymerase Chain Reaction; Sirt1: sirtuin-1; TAA: thioacetamide; TPO: Thrombopoietin; vGlut1: vesicular glutamate transporter 1; WFT: water-finding task; YM: Y-maze

Declarations

Ethics approval

The study was approved by the Ethics Committee of the First Affiliated Hospital of Wenzhou Medical University.

Consent to publication

Not applicable

Availability of data and material

The data that support the findings of this study are available from the corresponding author upon reasonable request.

Competing interests

The authors have declared no conflict of interest.

Funding

This study was supported by Basic Scientific Research Projects of Wenzhou city (Y20180076)Natural Science Foundation of Zhejiang province (LY21H030012) and Natural Science Foundation of China (81671042, 81300308).

Authors' Contributions

Saidan Ding supervised the entire project and designed the research. Shuya Feng and Baihui Chen conceived and designed the experiments, performed the research interpreted, and analysed the data, and wrote the paper. Xuebao Wang and Weikan Wang conceived and designed the experiments, interpreted and analysed the data, and supervised all the experimental procedure. Leping Liu, He Yu and Ruimin You performed the research and analysed the data. Xiaoai Lu, and Saidan Ding analysed the data and critically revised the manuscript. All authors read and approved the final manuscript.

Acknowledgments

We thank Dr. Haoqi Ni for optimizing the image analysis method. We thank Dr. Yangping Shentu for technical supports. We thank Dr. Yunchang Mo for critical reading of the manuscript.

References

1. Ehrenreich, H.*, et al.* A hematopoietic growth factor, thrombopoietin, has a proapoptotic role in the brain. *Proc Natl Acad Sci U S A***102**, 862-867 (2005).
2. Yang, M.*, et al.* Identification of TPO receptors on central nervous system-a preliminary report. *Zhongguo Shi Yan Xue Ye Xue Za Zhi***12**, 494-497 (2004).
3. Li, L.*, et al.* c-Mpl and TPO expression in the human central nervous system neurons inhibits neuronal apoptosis. *Aging (Albany NY)***12**, 7397-7410 (2020).
4. Wu, W.*, et al.* Thrombopoietin could protect cerebral tissue against ischemia-reperfusion injury by suppressing NF-κB and MMP-9 expression in rats. *Int J Med Sci***15**, 1341-1348 (2018).
5. Dame, C.*, et al.* Thrombopoietin gene expression in the developing human central nervous system. *Brain Res Dev Brain Res***143**, 217-223 (2003).
6. Columbyova, L., Loda, M. & Scadden, D.T. Thrombopoietin receptor expression in human cancer cell lines and primary tissues. *Cancer research***55**, 3509-3512 (1995).
7. Ivanova, A.*, et al.* Expression pattern of the thrombopoietin receptor (Mpl) in the murine central nervous system. *BMC developmental biology***10**, 77 (2010).
8. Li, B., Pan, H., Winkelmann, J.C. & Dai, W. Thrombopoietin and its alternatively spliced form are expressed in human amygdala and hippocampus. *Blood***87**, 5382-5384 (1996).
9. Bajaj, J.S.*, et al.* The effect of fatigue on driving skills in patients with hepatic encephalopathy. *The American journal of gastroenterology***104**, 898-905 (2009).
10. Sharma, P., Sharma, B.C., Puri, V. & Sarin, S.K. Critical flicker frequency: diagnostic tool for minimal hepatic encephalopathy. *Journal of hepatology***47**, 67-73 (2007).

11. Burness, C.B., Keating, G.M. & Garnock-Jones, K.P. Eltrombopag: A Review in Paediatric Chronic Immune Thrombocytopenia. *Drugs***76**, 869-878 (2016).
12. Cancello, R.*, et al.* Reduction of macrophage infiltration and chemoattractant gene expression changes in white adipose tissue of morbidly obese subjects after surgery-induced weight loss. *Diabetes***54**, 2277-2286 (2005).
13. Halberg, N.*, et al.* Hypoxia-inducible factor 1alpha induces fibrosis and insulin resistance in white adipose tissue. *Molecular & Cellular Biology***29**, 4467 (2009).
14. Krishnan, J.*, et al.* Dietary obesity-associated Hif1α activation in adipocytes restricts fatty acid oxidation and energy expenditure via suppression of the Sirt2-NAD+ system. *Genes & Development***26**, 259-270 (2012).
15. Lee, K.Y., Gesta, S., Boucher, J., Wang, X.L. & Kahn, C.R. The Differential Role of Hif1β/Arnt and the Hypoxic Response in Adipose Function, Fibrosis, and Inflammation. *Cell Metabolism***14**, 491-503 (2011).
16. Semenza, G.L. HIF-1: mediator of physiological and pathophysiological responses to hypoxia. *Journal of Applied Physiology***88**, 1474-1480 (2000).
17. Keith, B., Johnson, R.S. & Simon, M.C. HIF1α and HIF2α: sibling rivalry in hypoxic tumour growth and progression. *Nature Reviews Cancer***12**, 9 (2011).
18. Ding, S.*, et al.* Insulin Resistance Disrupts the Interaction Between AKT and the NMDA Receptor and the Inactivation of the CaMKIV/CREB Pathway in Minimal Hepatic Encephalopathy. *Toxicological sciences : an official journal of the Society of Toxicology***161**, 208 (2018).
19. Albrecht, J.*, et al.* Extracellular concentrations of taurine, glutamate, and aspartate in the cerebral cortex of rats at the asymptomatic stage of thioacetamide-induced hepatic failure: modulation by ketamine anesthesia. *Neurochemical research***25**, 1497-1502 (2000).
20. Yamada, M.*, et al.* Implanted cannula-mediated repetitive administration of Abeta25-35 into the mouse cerebral ventricle effectively impairs spatial working memory. *Behav. Brain Res.***164**, 139-146 (2005).
21. Kawasumi, M.*, et al.* Targeted introduction of V642I mutation in amyloid precursor protein gene causes functional abnormality resembling early stage of Alzheimer's disease in aged mice. *Eur. J. Neurosci.***19**, 2826-2838 (2004).
22. Takikawa, A.*, et al.* HIF-1α in Myeloid Cells Promotes Adipose Tissue Remodeling Toward Insulin Resistance. *Diabetes*, db160012 (2016).
23. Dokken, B.B., Sloniger, J.A. & Henriksen, E.J. Acute selective glycogen synthase kinase-3 inhibition enhances insulin signaling in prediabetic insulin-resistant rat skeletal muscle. *Am J Physiol Endocrinol Metab***288**, 1188-1194 (2005).
24. Mottet, D.*, et al.* Regulation of hypoxia-inducible factor-1alpha protein level during hypoxic conditions by the phosphatidylinositol 3-kinase/Akt/glycogen synthase kinase 3beta pathway in HepG2 cells. *Journal of Biological Chemistry***278**, 31277-31285 (2003).

25. Sun, C.*, et al.* SIRT1 Improves Insulin Sensitivity under Insulin-Resistant Conditions by Repressing PTP1B. *Cell Metabolism***6**, 307-319 (2007).
26. Satoh, A.*, et al.* SIRT1 promotes the central adaptive response to diet restriction through activation of the dorsomedial and lateral nuclei of the hypothalamus. *Journal of Neuroscience***30**, 10220-10232 (2010).
27. Matarese, G.*, et al.* Hunger-promoting hypothalamic neurons modulate effector and regulatory T-cell responses. *Proceedings of the National Academy of Sciences***110**, 6193-6198 (2013).
28. Chang, H.-C. & Guarente, L. SIRT1 mediates central circadian control in the SCN by a mechanism that decays with aging. *Cell***153**, 1448-1460 (2013).
29. Kaushansky, K. Thrombopoietin and the hematopoietic stem cell. *Blood***92**, 1-3 (1998).
30. Li, B. & Dai, W. Thrombopoietin and neurotrophins share a common domain. *Blood***86**, 1643-1644 (1995).
31. Methia, N., Louache, F., Vainchenker, W. & Wendling, F. Oligodeoxynucleotides antisense to the proto-oncogene c-mpl specifically inhibit in vitro megakaryocytopoiesis. *Blood***82**, 1395-1401 (1993).
32. Woodgett, J.R. Molecular cloning and expression of glycogen synthase kinase-3/factor A. *Embo Journal***9**, 2431-2438 (1990).
33. Roach, P.J. Control of glycogen synthase by hierarchal protein phosphorylation. *Faseb Journal Official Publication of the Federation of American Societies for Experimental Biology***4**, 2961 (1990).
34. Zhang, W.M., Depaoliroach, A.A. & Roach, P.J. Mechanisms of Multisite Phosphorylation and Inactivation of Rabbit Muscle Glycogen Synthase. *Archives of Biochemistry & Biophysics***304**, 219-225 (1993).
35. Henriksen, E.J. & Dokken, B.B. Role of glycogen synthase kinase-3 in insulin resistance and type 2 diabetes. *Current Drug Targets***7**, 1435 (2006).
36. Nikoulina, S.E.*, et al.* Potential role of glycogen synthase kinase-3 in skeletal muscle insulin resistance of type 2 diabetes. *Diabetes***49**, 263 (2000).
37. Rao, R.*, et al.* Glycogen synthase kinase 3 inhibition improves insulin-stimulated glucose metabolism but not hypertension in high-fat-fed C57BL/6J mice. *Diabetologia***50**, 452-460 (2007).
38. Henriksen, E.J. & Teachey, M.K. Short-term in vitro inhibition of glycogen synthase kinase 3 potentiates insulin signaling in type I skeletal muscle of Zucker Diabetic Fatty rats. **56**, 931-938 (2007).
39. Nikoulina, S.E.*, et al.* Inhibition of glycogen synthase kinase 3 improves insulin action and glucose metabolism in human skeletal muscle. *Diabetes***51**, 2190 (2002).
40. Broekaert, D.*, et al.* Comparison of leptin- and interleukin-6-regulated expression of the rPAP gene family: evidence for differential co-regulatory signals. *European Cytokine Network***13**, 78 (2002).
41. Xuan, O., Man, R.L., Huang, X., Messina-Graham, S. & Broxmeyer, H.E. SIRT1 Positively Regulates Autophagy and Mitochondria Function in Embryonic Stem Cells Under Oxidative Stress. *Stem Cells***32**, 1183–1194 (2014).

42. Szkudelski, T. & Szkudelska, K. Anti-diabetic effects of resveratrol. *Annals of the New York Academy of Sciences***1215**, 34–39 (2011).
43. Chao, J., Yu, M., Ys, Wang, M. & Chang, R. Dietary oxyresveratrol prevents parkinsonian mimetic 6-hydroxydopamine neurotoxicity. *Free Radical Biology & Medicine***45**, 1019-1026 (2008).
44. Pulla, V.K., Battu, M.B., Alvala, M., Sriram, D. & Yogeeswari, P. Can targeting SIRT-1 to treat type 2 diabetes be a good strategy? A review. *Expert Opinion on Therapeutic Targets***16**, 819-832 (2012).
45. Wang, R.H.*, et al.* Hepatic Sirt1 deficiency in mice impairs mTorc2/Akt signaling and results in hyperglycemia, oxidative damage, and insulin resistance. *Journal of Clinical Investigation***121**, 4477-4490 (2011).
46. Yoshizaki, T.*, et al.* SIRT1 Exerts Anti-Inflammatory Effects and Improves Insulin Sensitivity in Adipocytes. *Molecular & Cellular Biology***29**, 1363 (2009).
47. Milne, J.C. & Denu, J.M. The Sirtuin family: therapeutic targets to treat diseases of aging. *Current Opinion in Chemical Biology***12**, 11-17 (2008).
48. Milne, J.C.*, et al.* Small molecule activators of SIRT1 as therapeutics for the treatment of type 2 diabetes. *Nature***450**, 712-716 (2011).
49. Moynihan, K.A.*, et al.* Increased dosage of mammalian Sir2 in pancreatic beta cells enhances glucose-stimulated insulin secretion in mice. *Cell Metabolism***2**, 105-117 (2005).
50. Kim, D.*, et al.* SIRT1 deacetylase protects against neurodegeneration in models for Alzheimer's disease and amyotrophic lateral sclerosis. *Embo Journal***26**, 3169-3179 (2007).
51. Gao, J.*, et al.* A novel pathway regulates memory and plasticity via SIRT1 and miR-134. *Nature***466**, 1105-1109 (2010).
52. Donmez, G., Wang, D., Cohen, D.E. & Guarente, L. SIRT1 Suppresses β-Amyloid Production by Activating the α-Secretase Gene ADAM10. *Cell***142**, 320-332 (2010).
53. Donmez, G.*, et al.* SIRT1 protects against α-synuclein aggregation by activating molecular chaperones. *Journal of Neuroscience the Official Journal of the Society for Neuroscience***32**, 124-132 (2012).
54. Jeong, H.*, et al.* Sirt1 mediates neuroprotection from mutant huntingtin by activation of the TORC1 and CREB transcriptional pathway. *Nature Medicine***18**, 159-165 (2011).
55. Han, S., Choi, J.R., Soon, S.K. & Kang, S.J. Resveratrol upregulated heat shock proteins and extended the survival of G93A-SOD1 mice. *Brain Research***1483**, 112–117 (2012).
56. Fonseca-Kelly, Z.*, et al.* Resveratrol neuroprotection in a chronic mouse model of multiple sclerosis. *Frontiers in Neurology***3**, 84 (2012).
57. Michán, S.*, et al.* SIRT1 is essential for normal cognitive function and synaptic plasticity. *Journal of Neuroscience***30**, 9695-9707 (2010).
58. Dietrich, M.O.*, et al.* Agrp neurons mediate Sirt1's action on the melanocortin system and energy balance: roles for Sirt1 in neuronal firing and synaptic plasticity. *Journal of Neuroscience***30**, 11815-11825 (2010).

59. Lin, L.F., Doherty, D.H., Lile, J.D., Bektesh, S. & Collins, F. GDNF: a glial cell line-derived neurotrophic factor for midbrain dopaminergic neurons. *Science***260**, 1130-1132 (1993).
60. Lin, L.F., Zhang, T.J., Collins, F. & Armes, L.G. Purification and initial characterization of rat B49 glial cell line-derived neurotrophic factor. *Journal of Neurochemistry***63**, 758–768 (1994).
61. Lang, A.E.*, et al.* Randomized controlled trial of intraputamenal glial cell line-derived neurotrophic factor infusion in Parkinson disease. *Annals of Neurology***9**, 589-595 (2003).
62. Pertusa, M.*, et al.* Expression of GDNF transgene in astrocytes improves cognitive deficits in aged rats. *Neurobiology of Aging***29**, 1366-1379 (2008).
63. Du, F., Wang, L., Qian, W. & Liu, S. Loss of enteric neurons accompanied by decreased expression of GDNF and PI3K/Akt pathway in diabetic rats. *Neurogastroenterology & Motility the Official Journal of the European Gastrointestinal Motility Society***21**, 1229–e1114 (2009).
64. Pyo, H., Jou, I., Jung, S., Hong, S. & Joe, E.H. Mitogen-activated protein kinases activated by lipopolysaccharide and beta-amyloid in cultured rat microglia. *Neuroreport***9**, 871-874 (1998).
65. Savage, M.J., Lin, Y.G., Ciallella, J.R., Flood, D.G. & Scott, R.W. Activation of c-Jun N-terminal kinase and p38 in an Alzheimer's disease model is associated with amyloid deposition. *Journal of Neuroscience the Official Journal of the Society for Neuroscience***22**, 3376 (2002).

Tables

Table 1: The effects of ELT administration on insulin resistance in MHE groups of rats

Groups	Fasting plasma glucose (mg/dl)	Plasma insulin (ng/ml)	HOMA-IR
Control	108.3±20.57	1.8±0.31	8.1±1.01
MHE	170.7±22.68**	4.3±0.97**	39.6±3.71**
MHE+5ELT	167.7±19.91	4.1±0.82	38.4±2.27
MHE+25ELT	111.6±12.34##	1.9±0.28##	8.3±1.49##

*P<0.05, **P<0.01 vs Con group. #P <0.05, ##P <0.01 vs MHE group.

Figures

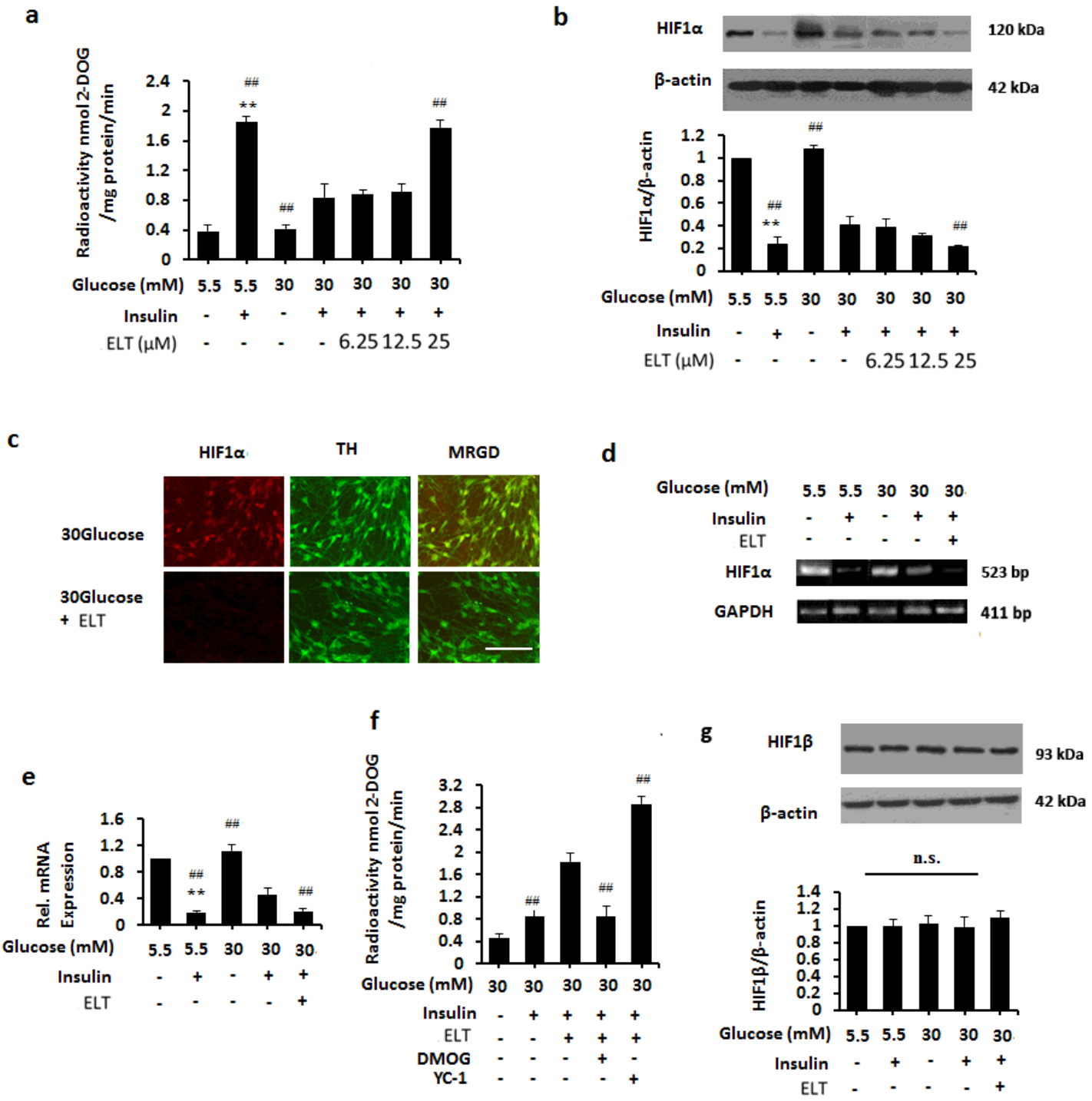

Figure 1

ELT reduced Insulin -mediated HIF1α in insulin resistant PHNs (a) Measurement of 2-NBDG uptake for PHNs treated with or without various concentration of ELT (6.25, 12.5 and 25 μM) after preincubation of 5.5 mM or 30mM glucose in the absence or presence of 100 nM insulin. Data are shown as mean± SD. *P <0.05, **P <0.01 vs 5.5 mM glucose -treated group. #P <0.05, ##P <0.01 vs 30mM glucose+100nM insulin -treated group. (b) IB analysis of lysate from PHNs treated with 5.5 mM or 30mM glucose after preincubation of various concentration of ELT (6.25, 12.5 and 25 μM) in the absence or presence of 100

nM insulin using anti-HIF1α and anti-β-actin antibodies and subsequent densitometry. (c) Double immunofluorescence staining of PHNs treated with 30mM glucose after preincubation with ELT (25 μM) in the absence or presence of 100 nM insulin using antibodies against HIF1α (Red), TH (Green). (d, e) RT-PCR (d) or Q-PCR (e) analysis of HIF1α mRNAs of PHNs treated with 5.5 mM or 30mM glucose after preincubation of 25 μM ELT in the absence or presence of 100 nM insulin. (f) Measurement of 2-NBDG uptake for PHNs treated with DMOG or YC-1 after preincubation of 25 μM ELT in the presence of 5.5 mM or 30mM glucose together with 100 nM insulin. (g) IB analysis of lysate from PHNs treated with 5.5 mM or 30 mM glucose after preincubation of ELT (25 μM) in the absence or presence of 100 nM insulin using anti-HIF1β and anti-β-actin antibodies and subsequent densitometry. Data are shown as mean± SD. *P <0.05, **P <0.01 vs 5.5 mM glucose -treated group. #P <0.05, ##P <0.01 vs 30mM glucose+100nM insulin -treated group. n.s., not significant. Scale bar, 25 μm.

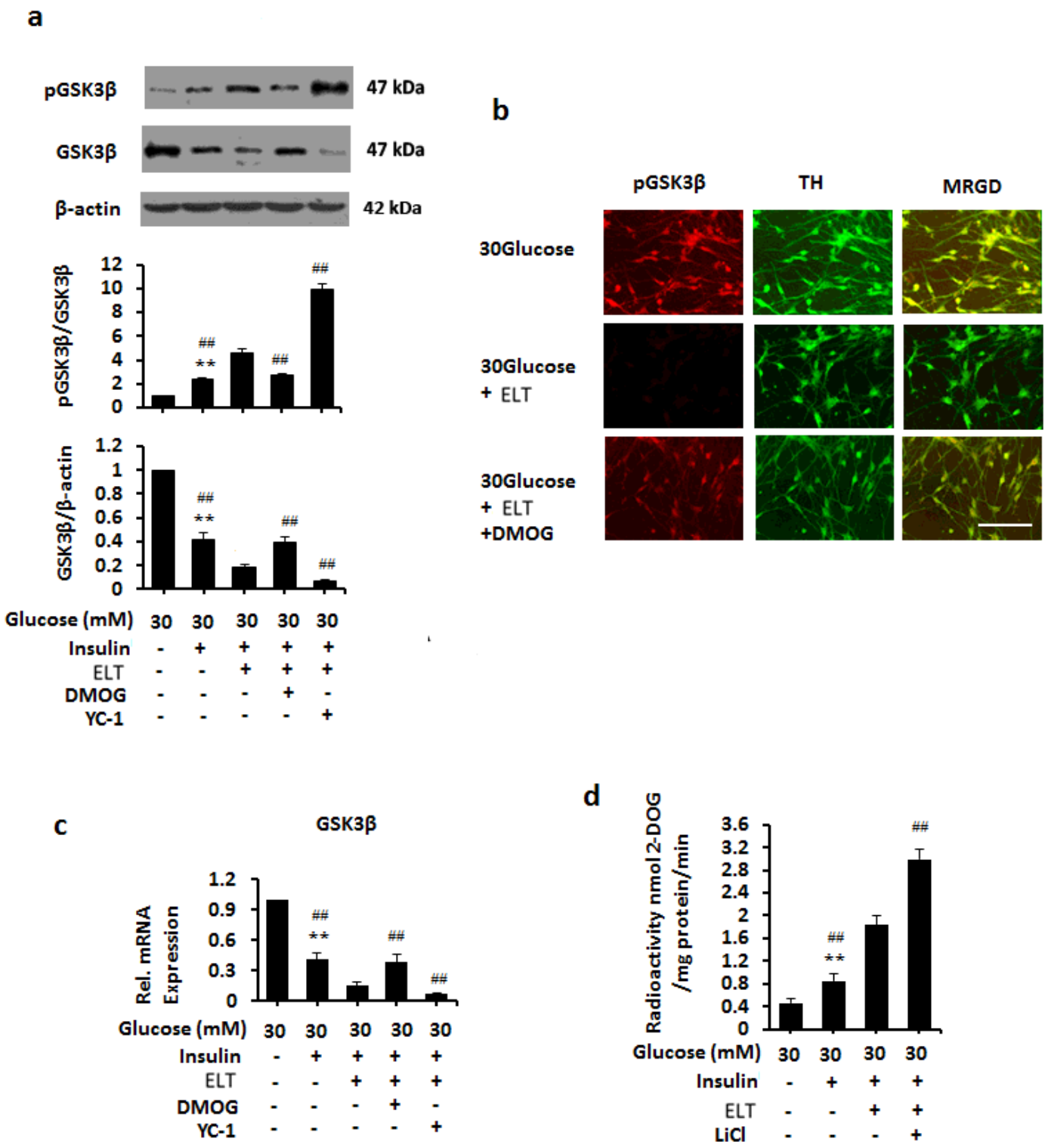

Figure 2

ELT increased insulin-mediated phosphorylation of GSK3β via HIF1α in insulin resistant PHNs (a) IB analysis of PHNs treated with DMOG or YC-1 after preincubation with 25 μM ELT in the presence of 30mM glucose together with 100 nM insulin using anti-pGSK3β/GSK3β and anti-β-actin antibodies and subsequent densitometry. (b) Double immunofluorescence staining of PHNs treated with DMOG after preincubation with 25 μM ELT in the presence of 30mM glucose together with 100 nM insulin using

antibodies against pGSK3β (red), MAP2 (green). (c) RT-PCR analysis of GSK3β mRNAs of PHNs treated with DMOG or YC-1 after preincubation with 25 μM ELT in the presence of 30mM glucose. (d) Measurement of 2-NBDG uptake for PHNs treated with LiCl after preincubation with 25 μM ELT in the presence of 30mM glucose together with or without 100 nM insulin. Data are shown as mean± SD. *P <0.05, **P <0.01 vs 30mM glucose-treated group. #P <0.05, ##P <0.01 vs 30mM glucose+ELT+100nM insulin -treated group. Scale bar, 25 μm.

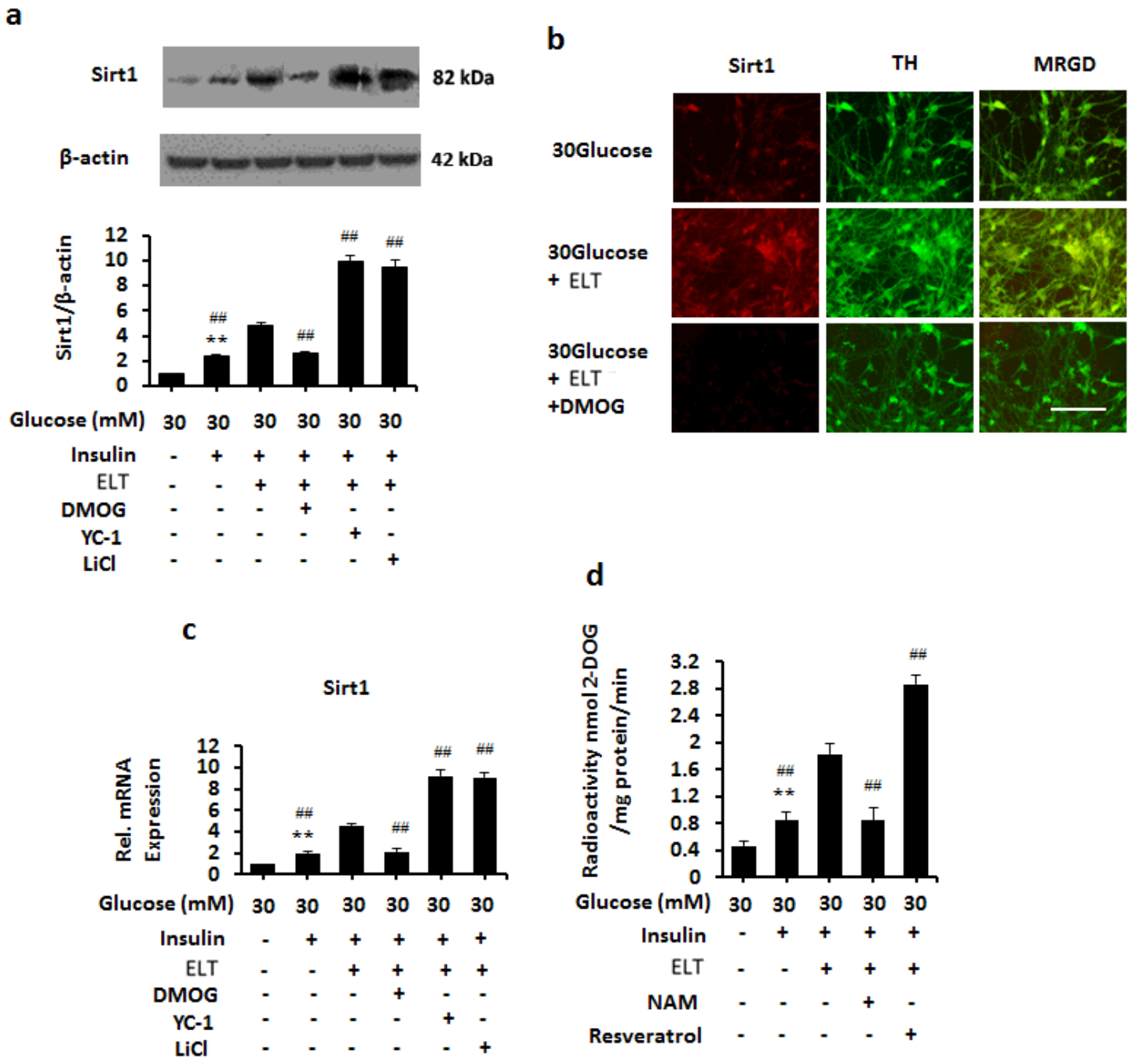

Figure 3

ELT increased insulin-mediated Sirt1 expression via HIF1α/GSK3β in insulin resistant PHNs (a) IB analysis of PHNs treated with DMOG/YC-1/LiCl after preincubation with 25 μM ELT in the presence of

30mM glucose together with or without 100 nM insulin using antibodies against Sirt1 and anti-β-actin and subsequent densitometry. (b) Double immunofluorescence staining of PHNs treated with DMOG after preincubation with 25 μM ELT in the presence of 30mM glucose together with 100 nM insulin using antibodies against Sirt1(Red), TH (Green). (c) RT-PCR analysis of GSK3β mRNAs of PHNs treated with DMOG/YC-1/LiCl after preincubation with 25 μM ELT in the presence of 30mM glucose. (d) Measurement of 2-NBDG uptake for PHNs treated with NAM or resveratrol after preincubation of 25 μM ELT in the presence of 30mM glucose together with or without 100 nM insulin. Data are shown as mean± SD. *P <0.05, **P <0.01 vs 30mM glucose-treated group. #P <0.05, ##P <0.01 vs 30mM glucose+ELT+100nM insulin -treated group. Scale bar, 25 μm.

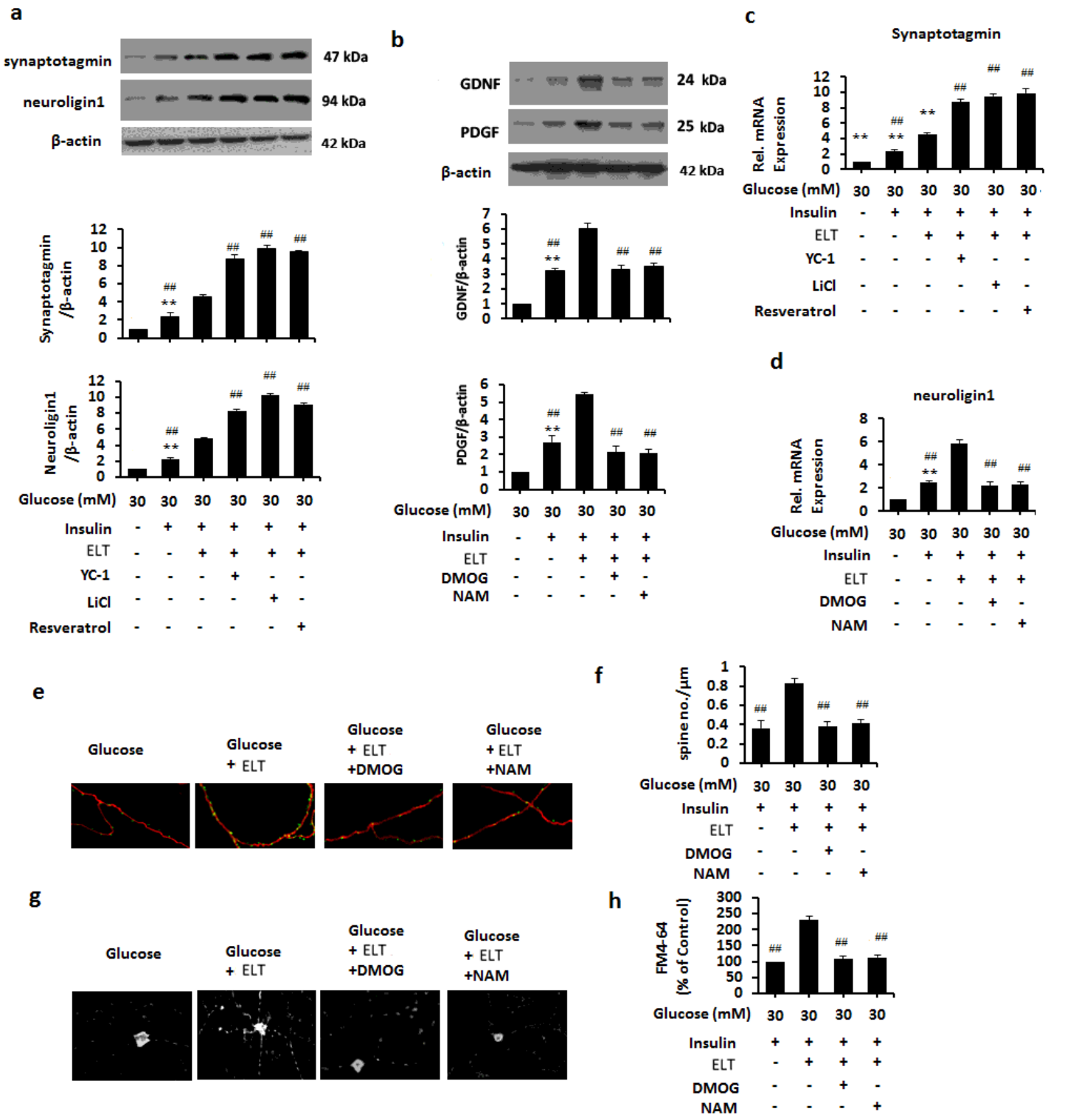

Figure 4

ELT increased insulin-mediated synaptic formation via HIF1α/GSK3β/Sirt1 in insulin resistant PHNs. (a) IB analysis of PHNs treated with YC-1/LiCl/ resveratrol preincubation of 25 μM ELT in the presence of 30mM glucose together with or without 100 nM insulin using antibodies against synaptotagmin/neuroligin1 and anti-β-actin and subsequent densitometry. (b) IB analysis of PHNs treated with DMOG/NAM after preincubation with 25 μM ELT in the presence of 30mM glucose together

with or without 100 nM insulin using antibodies against GDNF/PDGF and anti-β-actin and subsequent densitometry. (c) qPCR analysis of synaptotagmin mRNAs of PHNs treated with YC-1/LiCl/resveratrol preincubation with 25 μM ELT in the presence of 30mM glucose together with or without 100 nM insulin. (d) qPCR analysis of neuroligin1 mRNAs of PHNs treated with DMOG/NAM after preincubation with 25 μM ELT in the presence of 30mM glucose together with or without 100 nM insulin. (e) Immunostaining of PHNs treated with DMOG/NAM preincubation of 25 μM ELT in the presence of 30mM glucose together with or without 100 nM insulin against MAP2B (red) and vGluT1 (green). Red signals indicate MAP2B for microtubule staining and green signals indicate vGluT1 for detecting excitatory synapses. (f) Synaptic density was analyzed by counting green signals (vGluT1-positive dendriticspines) using ImageJ, and expressed per 1 μm of apical dendrite. (g) Representative image of FM4-64 staining of functional presynaptic terminals in PHNs treated with DMOG/NAM after preincubation of 25 μM ELT in the presence of 30mM glucose together with or without 100 nM insulin. The (h) panel indicates quantitative analysis of changes showed on average in FM4-64puncta intensity. Data are shown as mean± SD. *P<0.05, **P<0.01 vs 30mM glucose-treated group. #P <0.05, ##P <0.01 vs 30mM glucose+ELT+100nM insulin -treated group. Scale bar, 25 μm.

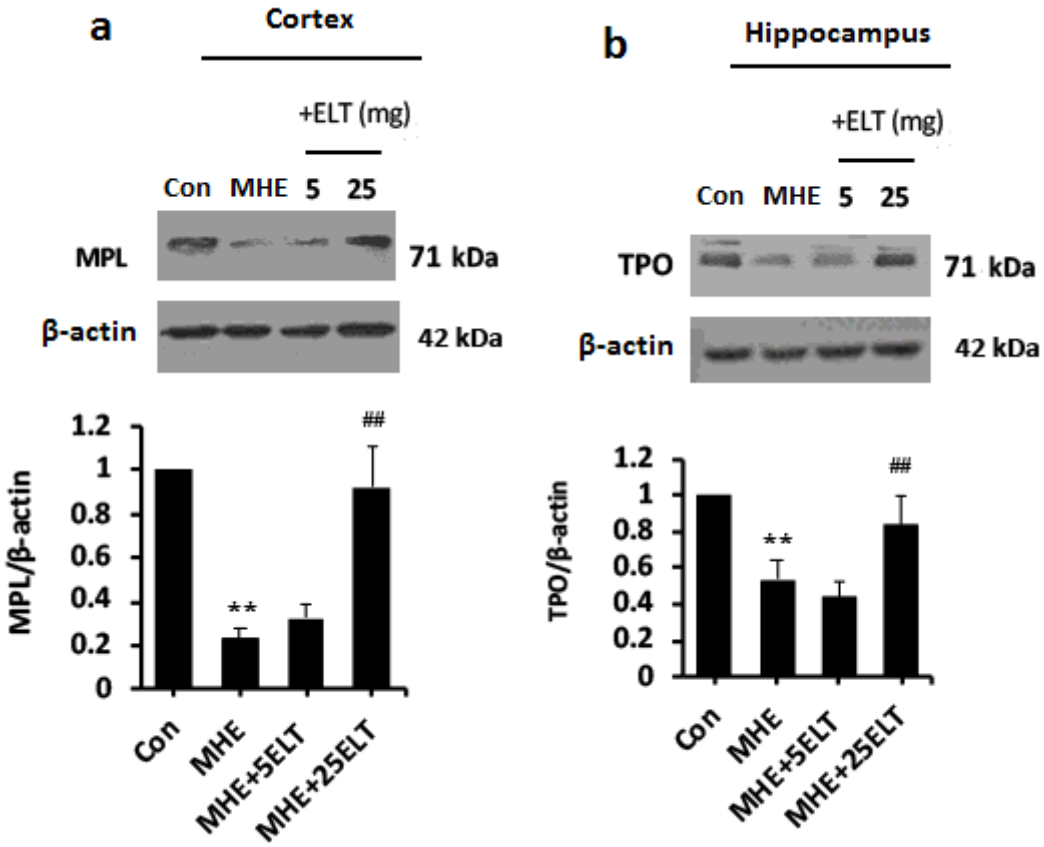

Figure 5

ELT increased MPL expression in MHE rats (a) IB analysis of cortical lysates from MHE rats administered with two dose (5, 25mg) of ELT using antibodies against MPL and β-actin and subsequent densitometry.

(b) IB analysis of hippocampal lysates from MHE rats administered with two dose (5, 25mg) of ELT using antibodies against TPO and β-actin and subsequent densitometry. Data are shown as mean± SD. *P <0.05, **P <0.01 vs Con group. #P <0.05, ##P <0.01 vs MHE model group. Scale bar, 25 μm. MRGD, merged image. Con, control.

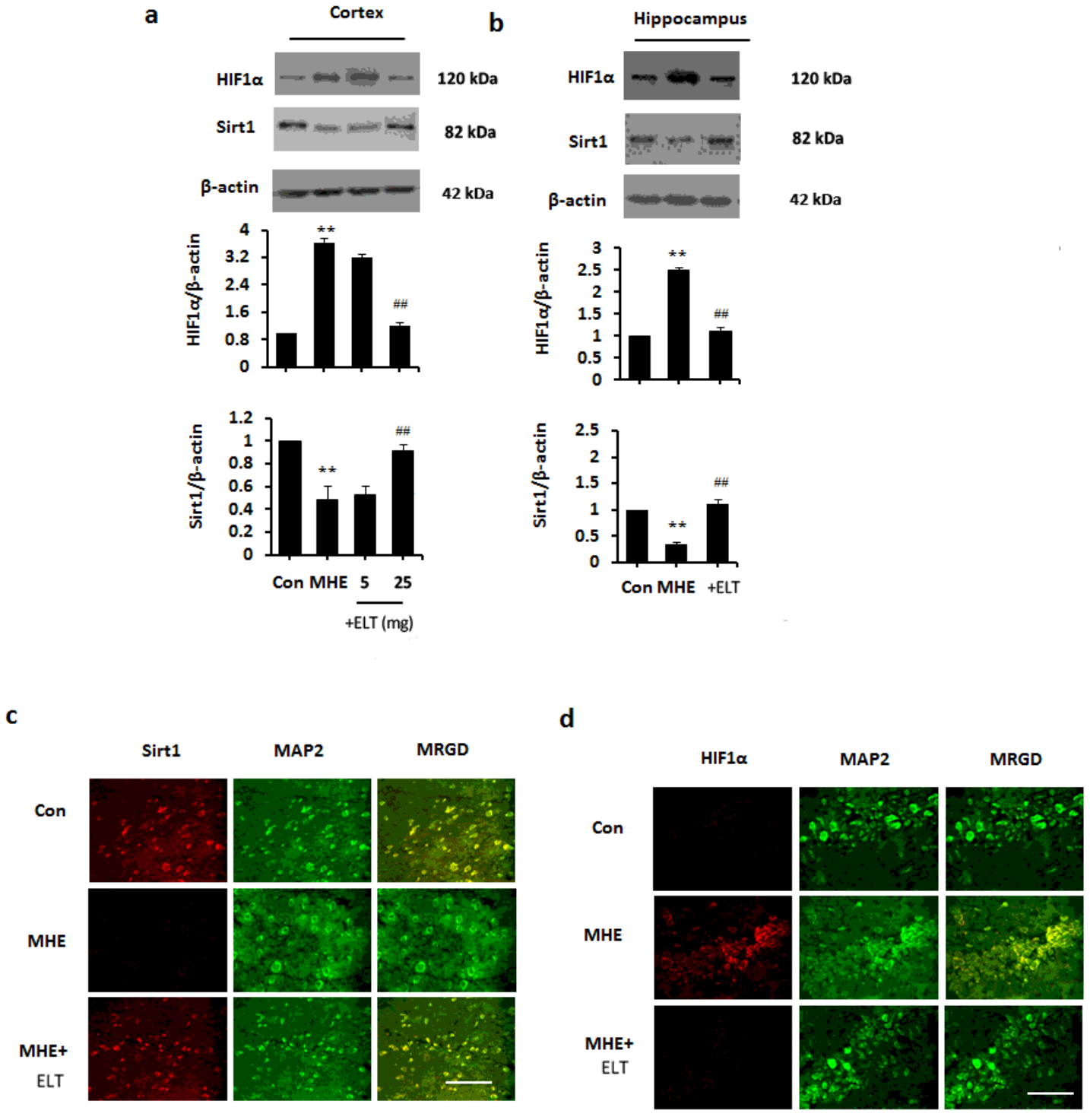

Figure 6

ELT improved HIF1α/Sirt1 signaling pathway in MHE rats (a) IB analysis of cortical homogenates from MHE rats administered with various concentrations of ELT (5, 25mg) using antibodies against

HIF1α/Sirt1 and β-actin and subsequent densitometry. (b) IB analysis of hippocampal homogenates from MHE rats after administration with 25mg ELT using antibodies against HIF1α/Sirt1 and β-actin and subsequent densitometry. (c) Immunostaining of free-floating cortical sections from MHE rats after administration with 25mg ELT using antibodies against Sirt1 (red) and MAP2 (green). (d) Immunostaining of free-floating hippocampal sections from MHE rats after administration with 25mg ELT using antibodies against HIF1α (red) and MAP2 (green). Data are shown as mean± SD. *P <0.05, **P <0.01 vs Con group. #P <0.05, ##P <0.01 vs MHE model group. Scale bar, 25 μm. MRGD, merged image. Con, control.

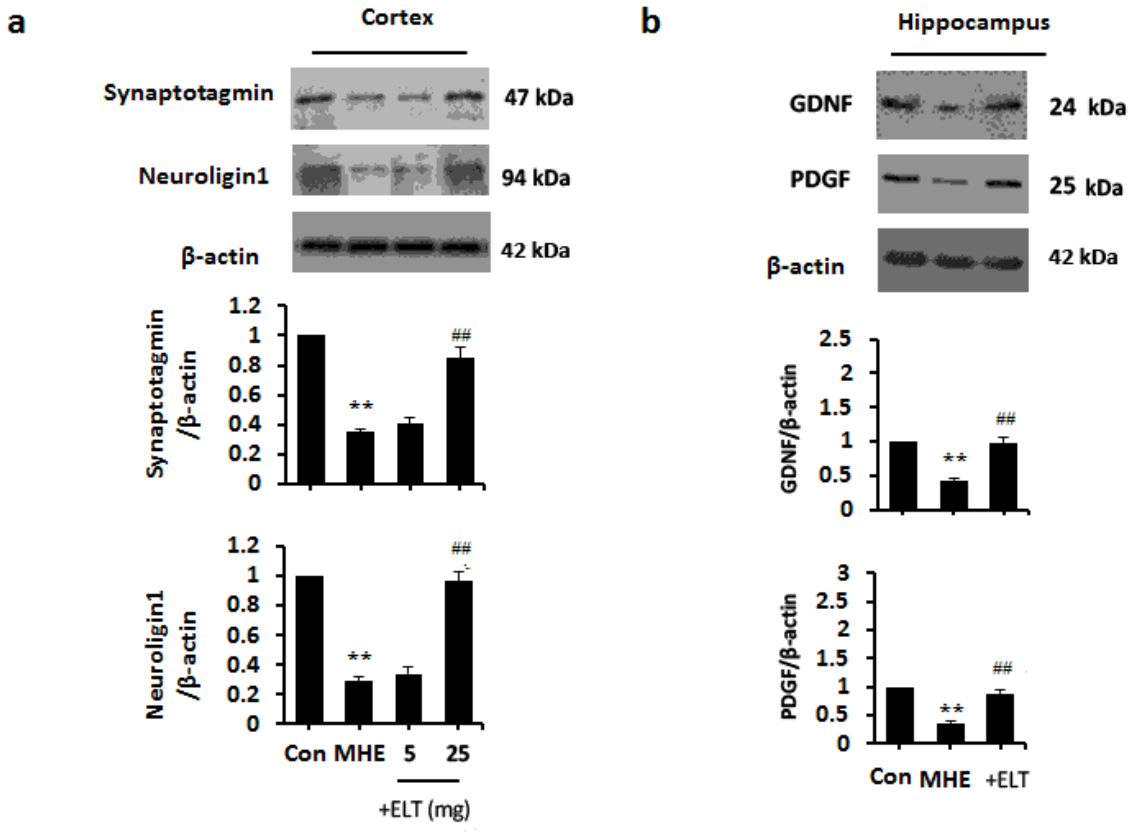

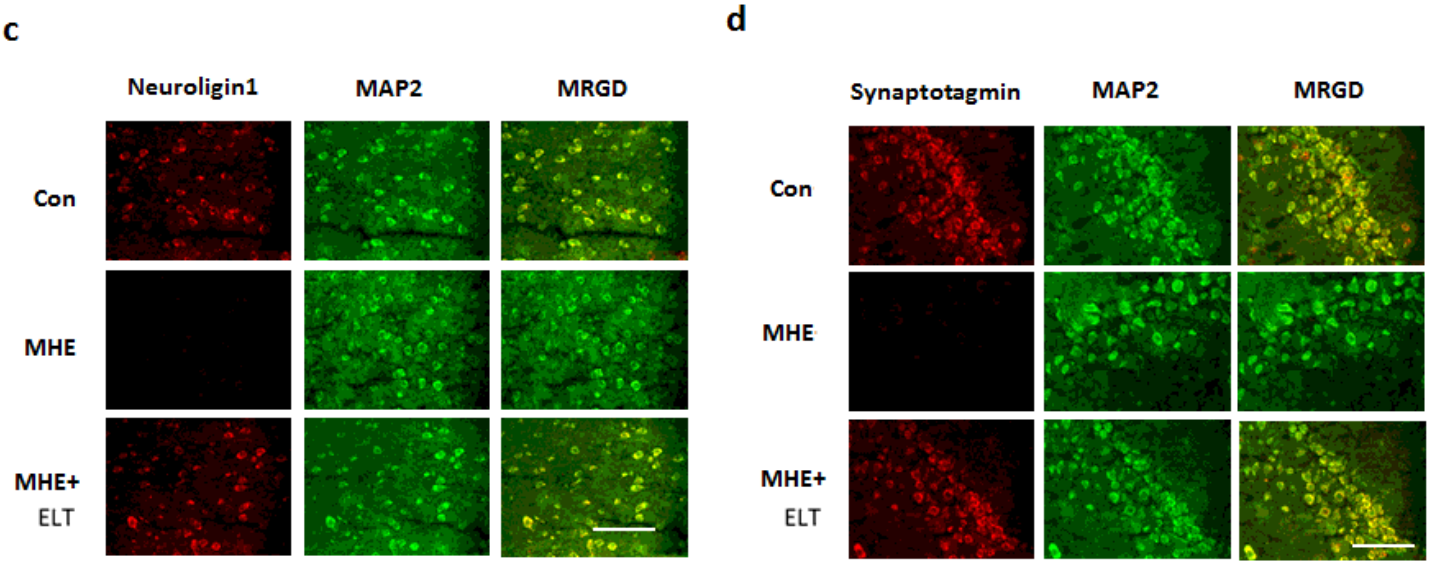

Figure 7

ELT improved destruction of synaptogenesis in MHE rats (a) IB analysis of cortical homogenates from MHE rats administered with various concentrations of ELT (5, 25mg) using antibodies against synaptotagmin/ neuroligin1 and β-actin and subsequent densitometry. (b) IB analysis of hippocampal homogenates from MHE rats after administration with 25mg ELT using antibodies against GDNF/PDGF and β-actin and subsequent densitometry. (c) Immunostaining of free-floating cortical sections from MHE rats after administration with 25mg ELT using antibodies against neuroligin (red) and MAP2 (green). (d) Immunostaining of free-floating hippocampal sections from MHE rats after administration with 25mg ELT using antibodies against synaptotagmin (red) and MAP2 (green). Scale bar, 25 μm. Data are shown as mean± SD. *P <0.05, **P <0.01 vs Con group. #P <0.05, ##P <0.01 vs MHE model group. Scale bar, 25 μm. MRGD, merged image. Con, control.

Supplementary Files

This is a list of supplementary files associated with this preprint. Click to download.

- FigureS1.tif
- FigureS2.tif